Numerical study on aero-optical imaging deviations of vehicles at different altitudes*

XU Liang[1], ZHANG Ziye[1], WANG Tao[2], WU Jianhui[3], and CHEN Xi[1]**

1. Tianjin Key Laboratory for Control Theory and Applications in Complicated Systems, School of Electrical Engineering and Automation, Tianjin University of Technology, Tianjin 300384, China

2. School of Intelligent Systems Engineering, Sun Yat-sen University, Guangzhou 510006, China

3. China Academy of Launch Vehicle Technology, Beijing 100076, China

(Received 25 May 2021; Revised 15 July 2021)

When the vehicle is flying in the atmosphere at high speed, the optical head and the atmosphere will have severe friction, thus forming a complex flow field, which makes the target image shift in the optical imaging system. The influence of altitude on aero-optical imaging deviation is studied in this paper. The geometric modeling and mesh generation of a typical blunt nosed high-speed vehicle were carried out, and the three-dimensional (3D) flow field density was obtained by a large amount of computational fluid dynamic calculation. In order to complete the optical calculation, the backward ray tracing method and the backward ray tracing stop criterion were used. The results show that as the height increases, the imaging deviation decreases gradually, and the imaging deviation slope increases and tends to be flat and close to zero.

Document code: A **Article ID:** 1673-1905(2022)02-0097-6

DOI https://doi.org/10.1007/s11801-022-1087-9

When a vehicle with optical imaging detection and guidance system is flying at high speed in the atmosphere, the target image received by the optical system is deviated from the actual position due to aero-optical effect[1], that is, the imaging deviation is generated. Imaging deviation will cause boresight error (BSE) and laser energy attenuation, which will lead to laser weapon efficiency reduction even failure. MILLER[2] discussed the factors affecting atmospheric interception, and believed that flight altitude and light of sight (LOS) angle were the main factors affecting aero-optical BSE. GIERLOFF and ROBERTSON et al[3] used computational fluid dynamic (CFD) and aero-optics software to give the BSE of a typical interceptor at an angle of attack of 0° at an altitude of 10—60 km (an interval of 10 km). XU et al[4-7] believed that the more uniform the flow field density distribution on light propagation path is, the smaller the imaging deviation will be, and conversely, the larger the deviation will be. YAO et al[8] proposed that with the increase of LOS angle, the aero-optical imaging deviation of blunt vehicle gradually decreases. WU et al[9] used an improved optimization algorithm to predict the aero-optical imaging deviation and evaluated the algorithm model using mean square error and coefficient of determination. WANG et al[10,11] numerically calculated the optical properties of the aero-optical flow field and gave the calculation results of optical path difference (OPD) and strehl ratio. WANG et al generated new physical understanding through numerical and experimental investigations, and these new physical understandings highlighted for a number of important aero-optical flows, including turbulent boundary layers, separated shear layers, and flow over optical turrets. And approaches for mitigating aero-optical effects are briefly discussed[12].

The image deviation generated by the high-speed flow field will affect the aiming accuracy of the aircraft and cause the hit error of the aiming point of the aircraft. Therefore, it is of great significance to calculate and compensate the aero-optical imaging deviation in real time. The laboratory can correct the aero-optical imaging deviation caused by the average density field to some extent, but in practical engineering, the problems caused by the imaging deviation have not been completely solved. The aero-optical flow field structure and flow field variables will change with the altitude, Mach number and angle of attack of the aircraft. We can carefully examine the imaging deviation rules of specific aircraft at different altitudes, different line of sight angles and different Mach numbers. On the one hand, it compensates the imaging deviation from the perspective of software, and on the other hand, it reduces the imaging deviation from the intersection angle and line of sight angle.

In this paper, the flight states of blunt aircraft are

* This work has been supported by the National Natural Science Foundation of China (Nos.61975151 and 61308120), and the Big Data Research Foundation of PICC (No.201900418CI000008).

** E-mail: liangx999@163.com

calculated at 0—25 km, 0.5—3 Mach, 0°—60° angle of attack, 5°—85° line of sight angle and 0°—90° line of sight roll angle. This paper studies the influence of altitudes within the range of 0—25 km on aero-optical imaging deviation. The fluid dynamics calculations were performed using the Reynolds-average Navier-Stokes solver provided by finite element software[13]. Runge-Kutta method was used to calculate the backward ray tracing, the imaging deviation of different altitudes was calculated, and the factors affecting the imaging deviation were analyzed.

BSE refers to the direction deviation of the centroid position of the target image in the presence or absence of interference, that is, the angle between the actual line of sight and the measured line of sight. The difference reflected in the image plane by the BSE is the imaging deviation. Because there are many sources of imaging deviation, the aero-optical flow field is separated from the whole propagation process and the light propagation is studied separately. That part of the aero-optical flow field is called aero-optical imaging deviation, which describes the deflecting effect of the aero-optical flow field on light propagation. In geometric optics, the image deviation of vehicle under different flight conditions can be obtained by ray tracing calculation.

The vehicle is flying at high altitude, it is surrounded by the non-uniform flow field, and outside the non-uniform flow field is atmosphere free stream. Take the airborne optical imaging system as an example, as shown in Fig.1. The light emanates from the target, and it first moves in a relatively straight line through a supposedly uniform free flow to reach the aero-optical flow field. Due to the effects of the aero-optics, the light will be deflected after passing through the aero-optical flow field, and there is a difference between the position of the light on the outside surface of the window and that without the aerodynamic optical flow field. Assuming that the outer surface of the window is taken as the imaging plane, there will be imaging bias on the plane, namely imaging deviation.

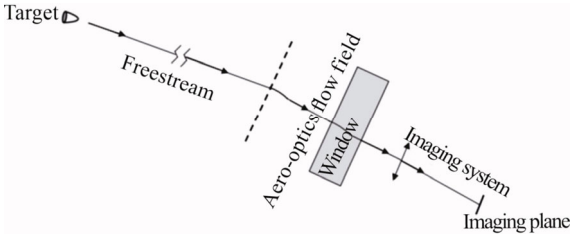

Fig.1 Aero-optical ray propagation process

CFD is a common method to study aero-optical effects, which can be used to calculate the complex flow field around vehicle[14,15]. The imaging deviation and imaging blur of aero-optical effects are the results of the average flow field. Therefore, it's natural to think of solving the time-averaged Navier Stokes equation to describe the flow field, which is the Reynolds average method.

Realizable k-ε two equation model is commonly used in Reynolds average method. In the realizable k-ε two equation model, turbulent kinetic energy k and dissipation rate ε are introduced[16], and the corresponding transport equation is

$$\frac{\partial(\rho k)}{\partial t}+\frac{\partial(\rho k u_i)}{\partial x_i}=\frac{\partial}{\partial x_j}\left[\left(\mu+\frac{\mu_t}{\sigma_k}\right)\frac{\partial k}{\partial x_j}\right]+G_k+G_b-\rho\varepsilon-Y_M-S_k, \tag{1}$$

$$\frac{\partial(\rho\varepsilon)}{\partial t}+\frac{\partial(\rho\varepsilon u_i)}{\partial x_i}=\frac{\partial}{\partial x_j}\left[\left(\mu+\frac{\mu_t}{\sigma_\varepsilon}\right)\frac{\partial \varepsilon}{\partial x_j}\right]+C_{1\varepsilon}\frac{\varepsilon}{k}\left(G_k+C_{3\varepsilon}G_b\right)-C_{2\varepsilon}\rho\frac{\varepsilon^2}{k}+S_\varepsilon, \tag{2}$$

where C_1, C_2 and C_3 are empirical constants, G_k is the production term of turbulent kinetic energy k caused by average velocity gradient, G_b is the production term of turbulent kinetic energy k caused by buoyancy, Y_M represents the contribution of pulsation expansion in compressible turbulence, σ_k and σ_ε are Prandtl numbers corresponding to turbulent kinetic energy k and dissipation rate ε, respectively, S_k and S_ε are user-defined source items, μ is hydrodynamic viscosity, and μ_t is turbulent viscosity.

Refractive index n is a very important parameter in optical display of atmospheric flow field. For normal temperature atmospheric flow field, the distribution of refractive index value usually depends on the distribution of gas density. After the flow field density distribution of discrete points is obtained through CFD calculation, Gladstone-Dale empirical formula is used to relate the refractive index and the density distribution as follows

$$n-1=K_{GD}\rho, \tag{3}$$

where n is the refractive index of the atmospheric flow field, ρ is the density of the atmospheric flow field, and K_{GD} is called Gladstone-Dale coefficient, which is a characteristic of gas, and the unit is m^3/kg.

Gladstone-Dale constant can be approximated as an empirical formula for the wavelength of light waves[17,18], as shown below

$$K_{GD}=2.23\times10^{-4}\left(1+7.52\times\frac{10^{-3}}{\lambda^2}\right), \tag{4}$$

where λ is the wavelength of light wave, and the unit is μm. Tab.1 lists the Gladstone-Dale coefficients corresponding to wavelengths from 0.4 μm to 0.6 μm. The wavelength λ calculated in this paper is 0.5 μm.

Tab.1 Relationship between Gladstone-Dale coefficient and wavelength

Wavelength (μm)	Gladstone-Dale coefficient (m^3/kg)
0.4	0.000 228 1
0.5	0.000 223 6
0.6	0.000 222 0

By substituting K_{GD} into Eq.(3), the relationship between optical refractive index field and density field can be obtained as follows

$$n=1+2.23\times10^{-4}\left(1+7.52\times\frac{10^{-3}}{\lambda^{-2}}\right)\cdot\rho. \tag{5}$$

Geometrical optics is very effective in the study of ray propagation in non-uniform media, so it is used in the study of aero-optical to calculate the propagation path deflection of ray in aerodynamic flow field. The optical propagation calculation method of geometric optics, namely ray tracing, is to track the path of ray propagation. Tracing is achieved by solving the equation that describes the path of ray propagation (ray equation).

The expression of the ray equation is

$$\frac{\mathrm{d}}{\mathrm{d}s}\left(n(\boldsymbol{r})\frac{\mathrm{d}\boldsymbol{r}}{\mathrm{d}s}\right)=\nabla n(\boldsymbol{r}), \tag{6}$$

where s is the arc length on the path of ray propagation, $\boldsymbol{r}$ is the space coordinate vector of the ray, n is the refractive index, $\nabla n(\boldsymbol{r})$ is a refractive index gradient at the ray location $\boldsymbol{r}$, and $\mathrm{d}\boldsymbol{r}/\mathrm{d}s$ is the tangential unit vector of light.

In this paper, the fourth-order Runge-Kutta method is used as ray tracing method[18,19].

Eq.(6) is not convenient for direct integration, so a new variable is introduced to change its form and is defined as

$$\mathrm{d}t=\frac{\mathrm{d}s}{n}. \tag{7}$$

Therefore, Eq.(6) can be simplified into the second order differential form as

$$\frac{\mathrm{d}^2\boldsymbol{r}}{\mathrm{d}t^2}=n\cdot\nabla n. \tag{8}$$

Define the ray vector as

$$\boldsymbol{T}=n\frac{\mathrm{d}\boldsymbol{r}}{\mathrm{d}s}. \tag{9}$$

Eq.(8) can be further transformed into the first order differential equations as

$$\begin{cases}\dfrac{\mathrm{d}\boldsymbol{r}}{\mathrm{d}t}=\boldsymbol{T}\\[2ex]\dfrac{\mathrm{d}\boldsymbol{T}}{\mathrm{d}t}=n\cdot\nabla n\end{cases}. \tag{10}$$

According to Runge-Kutta method of order 4, the numerical calculation formula of tracing ray is

$$\begin{cases}\boldsymbol{r}_1=\boldsymbol{r}_0+\dfrac{\Delta t}{6}\left(\boldsymbol{K}_1+2\boldsymbol{K}_2+2\boldsymbol{K}_3+\boldsymbol{K}_4\right)\\[2ex]\boldsymbol{T}_1=\boldsymbol{T}_0+\dfrac{\Delta t}{6}\left(\boldsymbol{L}_1+2\boldsymbol{L}_2+2\boldsymbol{L}_3+\boldsymbol{L}_4\right)\end{cases}, \tag{11}$$

where Δt is a ray trace step, $\boldsymbol{K}_1$ is the direction vector at the initial position $\boldsymbol{r}_0$ of the ray, and $\boldsymbol{L}_1$ is the product of refractive index and refractive index gradient vector at $\boldsymbol{r}_0$. $\boldsymbol{K}_2$ is the direction vector of the ray at $[\boldsymbol{r}_0+\Delta t\cdot(\boldsymbol{K}_1/2)]$ interpolated by the initial position, and $\boldsymbol{L}_2$ is the product of refractive index and refractive index gradient vector at $[\boldsymbol{r}_0+\Delta t\cdot(\boldsymbol{K}_1/2)]$. $\boldsymbol{K}_3$ is the direction vector at the initial position $[\boldsymbol{r}_0+\Delta t\cdot(\boldsymbol{K}_2/2)]$ of the ray, and $\boldsymbol{L}_3$ is the product of refractive index and refractive index gradient vector at $[\boldsymbol{r}_0+\Delta t\cdot(\boldsymbol{K}_2/2)]$. $\boldsymbol{K}_4$ is the direction vector at the initial position $[\boldsymbol{r}_0+\Delta t\cdot\boldsymbol{K}_3)]$ of the ray, and $\boldsymbol{L}_4$ is the product of refractive index and refractive index gradient vector at $[\boldsymbol{r}_0+\Delta t\cdot\boldsymbol{K}_3]$. There specific values are as follows

$$\begin{cases}\boldsymbol{K}_1=\boldsymbol{T}_0\\ \boldsymbol{L}_1=n\cdot\nabla n\end{cases}, \tag{12}$$

$$\begin{cases}\boldsymbol{K}_2=\boldsymbol{T}_0+\dfrac{t}{2}\boldsymbol{L}_1\\ \boldsymbol{L}_2=n\cdot\nabla n\end{cases}, \tag{13}$$

$$\begin{cases}\boldsymbol{K}_3=\boldsymbol{T}_0+\dfrac{\Delta t}{2}\boldsymbol{L}_2\\ \boldsymbol{L}_3=n\cdot\nabla n\end{cases}, \tag{14}$$

$$\begin{cases}\boldsymbol{K}_4=\boldsymbol{T}_0+\Delta t\boldsymbol{L}_3\\ \boldsymbol{L}_4=n\cdot\nabla n\end{cases}. \tag{15}$$

Given the initial position $\boldsymbol{r}_0$ and the initial incident direction $\boldsymbol{T}_0$ of the ray, $\boldsymbol{r}_1$ (position) and $\boldsymbol{T}_1$ (trajectory direction of the ray) at the end of the step size can be obtained, and these can be used as the initial conditions for the next step tracing. The whole process can be tracked gradually according to the step size Δt until the completion.

In this paper, a backward ray tracing method for aero-optical flow field is used, and quadrilateral mesh interpolation is used to calculate the refractive index and refractive index gradient of the next point in the ray tracing[18,20]. TA stop criterion is used to determine the end point of the backward ray-tracing, so that the ray-tracing stops at the boundary of the flow field.

In this paper, the optical head of high-speed vehicle is simplified to obtain the head model of blunt vehicle, as shown in Fig.2(a). The C-type computing grid is shown in Fig.2(b). The C-type grid computing area outside the head is large enough. The hexahedral grid was adopted, containing a total of 565 238 grid cells.

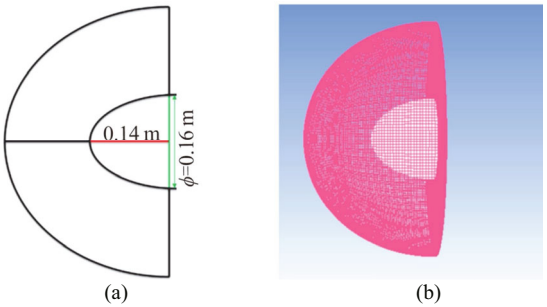

Fig.2 (a) Geometric dimensions and (b) C-type grid of the three-dimensional (3D) blunt model

As shown in Tab.2, four groups of different flight conditions are given to show the average flow field density, refractive index distribution, imaging deviation and imaging deviation slope of the vehicle at different altitudes of 0—25 km.

Tab.2 Flight condition

Sample	Mach number	Angle of attack	Line of sight roll angle	Line of sight angle
1	3	30°	30°	25°
2	3	60°	0°	75°
3	2	60°	60°	75°
4	2	0°	0°	25°

Fig.3 shows the geometric relationship between the vehicle and the target in the three-dimensional plane, where M represents the center of mass of the vehicle, T is the center of mass of the target, and M_{XYZ} refers to inertial coordinate system. The angle between the vehicle and the target in the horizontal direction represents the line of sight angle, expressed by α. The angle between the vehicle and the target in the vertical direction represents the line of sight roll angle, expressed by β.

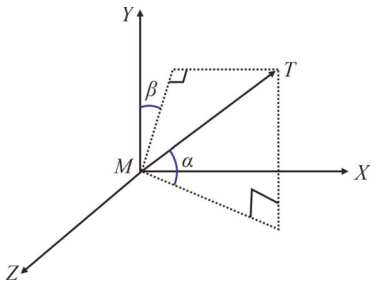

Fig.3 3D geometric relationship between the vehicle and the target

In this study, as shown in Fig.4 and Fig.5, the average flow field densities of two groups of different flight conditions were randomly selected from four groups of different flight conditions, showing the results of flow field density figures at different altitudes of 0—25 km. As can be seen from these figures, the flow field structure is similar at different altitudes. The average flow field density gradually decreases with the increase of altitude, which is consistent with the knowledge of aerodynamics.

Fig.6 shows the refractive index distribution of the backward ray-tracing of the vehicle at different altitudes. Where the abscissa is the normalized step size and the ordinate is the refractive index. The ray-tracing process is a free flow from inside the vehicle window into the atmosphere. First, it passes through the aero-optical flow field area of the vehicle head, where the density is higher, that is, the refractive index increases. Then from the aero-optical flow field area to the atmospheric free flow, the density of this section decreases, that is, the refractive index decreases.

Figs.7—10 shows the imaging deviation and imaging deviation slope of 3D blunt nosed aircraft under different flight conditions. As can be seen from the above figures, the curves in the four graphs show the same trend. With the increase of altitude, the imaging deviation decreases gradually. This result is consistent with the distribution law of aerodynamic optical flow field. That is, with the increase of the altitude, the density of the non-uniform flow field through the light propagation becomes sparse, and the refractive index decreases, and the imaging deviation decreases.

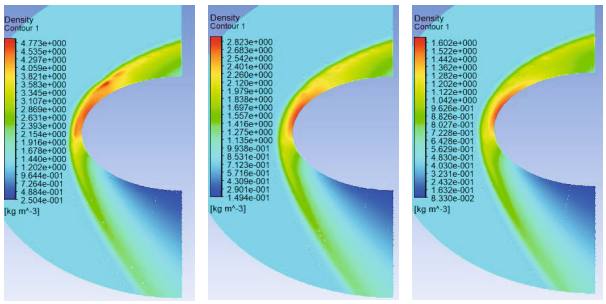

(a) 0 km (b) 5 km (c) 10 km

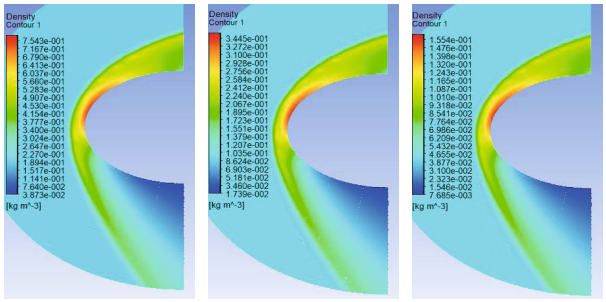

(d) 15 km (e) 20 km (f) 25 km

Fig.4 Average flow field density (Sample 1)

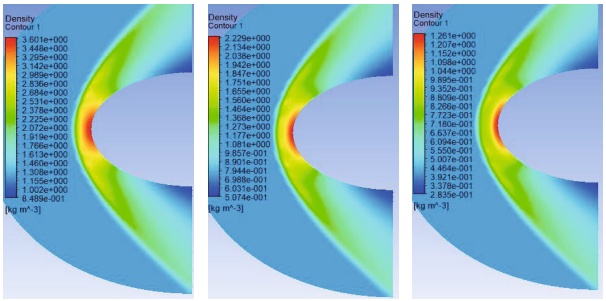

(a) 0 km (b) 5 km (c) 10 km

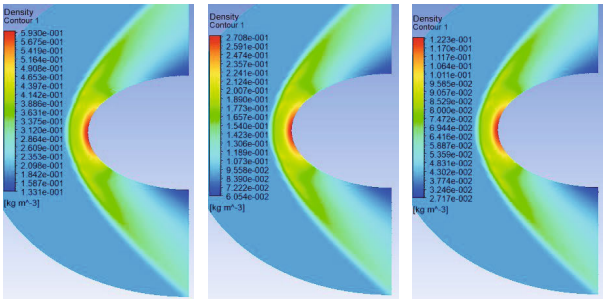

(d) 15 km (e) 20 km (f) 25 km

Fig.5 Average flow field density (Sample 4)

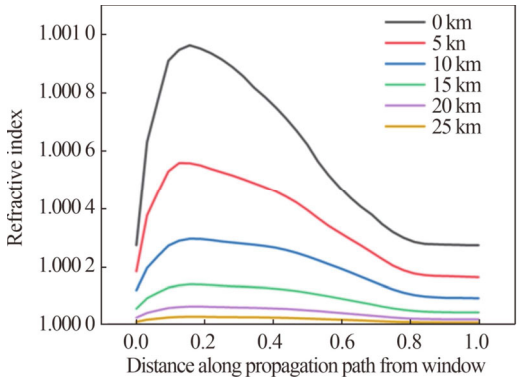

Fig.6 Refractive index distributions of backward ray tracing at different altitudes (Sample 1)

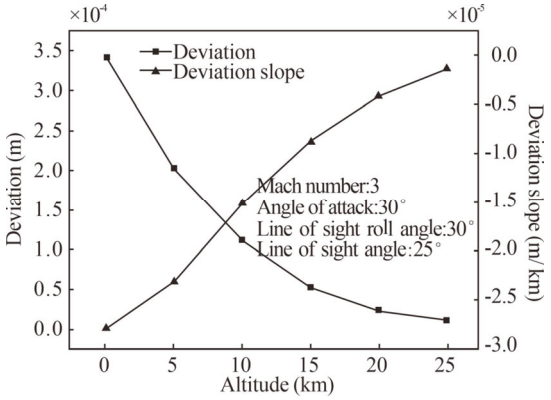

Fig.7 Imaging deviation and imaging deviation slope (Sample 1)

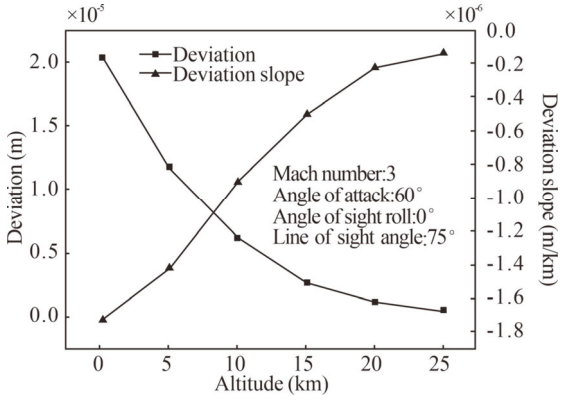

Fig.8 Imaging deviation and imaging deviation slope (Sample 2)

Imaging deviation slope is a critical parameter that affects system performance[6,8]. It is defined as the ratio of small changes in imaging deviation to changes in related variables over the same period of time.

The imaging deviation slope of the left boundary is expressed as

$$\nabla d = \frac{d_{i+1} - d_i}{\Delta x}. \tag{16}$$

The center imaging deviation slope is expressed as

$$\nabla d = \frac{d_{i+1} - d_{i-1}}{2\Delta x}. \tag{17}$$

The imaging deviation slope of the left boundary is expressed as

$$\nabla d = \frac{d_i - d_{i-1}}{\Delta x}, \tag{18}$$

where d is the imaging deviation, Δx is the step size of the change of relevant variable, which is 5 km altitude in this paper, and Δd is the imaging deviation slope.

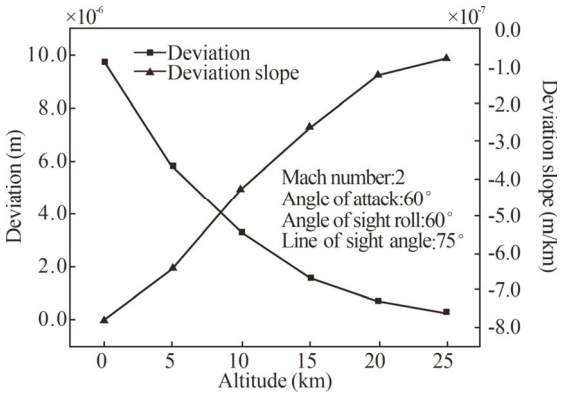

Fig.9 Imaging deviation and imaging deviation slope (Sample 3)

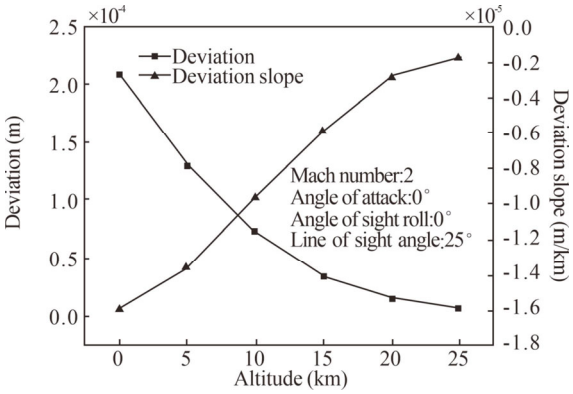

Fig.10 Imaging deviation and imaging deviation slope (Sample 4)

This paper mainly studies the influence of different altitudes on the aero-optical imaging deviation. The density distribution of the flow field outside the optical hood of the high-speed aircraft flying at an altitude of 0—25 km is calculated by FLUENT. By using Gladstone-Dale formula, the density field is converted into the refractive index field, and then the backward ray-tracing is realized. The results show that with the increase of altitude, the refractive index decreases gradually, and the aero-optical imaging deviation decreases gradually. At the same time, with the increase of altitude, the imaging deviation slope gradually approaches zero, that is, the change of lower altitude will cause larger imaging deviation.

Statements and Declarations

The authors declare that there are no conflicts of interest

related to this article.

References

[1] LI G C. Aero-optics[M]. Beijing：National Defense Industry Press, 2006. (in Chinese)

[2] MILLER D W. AIT interceptor performance predictions[C]//2nd Annual AIAA/SDIO Interceptor Technology Conference, June 6-9, 1993, Albuquerque, NM, America. Reston：AIAA, 1993.

[3] GIERLOFF J J, ROBERTSON S J, BOUSKA D H. Computer analysis of aero-optics effects[C]//The AIAA/SDIO Annual Interceptor Technology Conference, May 19-21, 1992, Huntsville, AL, America. Reston：AIAA, 1992.

[4] XU L, CAI Y L. High altitude aero-optic imaging deviation prediction for a hypersonic flying vehicle[C]//Proceedings of 2011 IEEE International Conference on Imaging Systems and Techniques, May 17-18, 2011, Batu Ferringhi, Malaysia. New York：IEEE, 2011：210-214.

[5] XU L, CAI Y L. Influence of non-uniform flow fields on imaging deviation of side-window airborne optical systems[C]//Proceedings of 2011 IEEE International Conference on Imaging Systems and Techniques, May 17-18, 2011, Batu Ferringhi, Malaysia. New York：IEEE, 2011：12-15.

[6] XU L, CAI Y L. Influence of altitude on aero-optic imaging deviation[J]. Applied optics, 2011, 50(18)：2949-2957.

[7] XU L, CAI Y L. Imaging deviation through non-uniform flow fields around high-speed flying vehicles[J]. Optik, 2012, 123(13)：1177-1182.

[8] YAO Y, XUE W, WANG T, et al. Influence of LOS angle on aero-optics imaging deviation[J]. Optik, 2019, 202(18)：163732.

[9] WU Y Y, XUE W, XU L, et al. Least-squares support vector machine for predicting aero-optic imaging deviation based on chaotic particle swarm optimization[J]. Optik, 2019, 206(12)：163215.

[10] WANG T, ZHAO Y, XU D. Numerical study using angular spectrum propagation model for aero optical imaging[J]. Optik, 2013, 124(5)：411-415.

[11] WANG T, ZHAO Y, XU D, et al. Numerical study of evaluating the optical quality of supersonic flow fields[J]. Applied optics, 2007, 46(23)：5545-5551.

[12] WANG M, MANI A, GORDEYEV S. Physics and computation of aero-optics[J]. Annual review of fluid mechanics, 2012, 44(1)：299-321.

[13] WANG X Q, SARHADDI D, WANG Z, et al. Modeling-based hyper-reduction of multidimensional computational fluid dynamics data：application to ship airwake data[J]. Journal of aircraft, 2019, 56(6)：1-12.

[14] XU D, LIU H W, WU L, et al. High-order singular value decomposition applied in aero-optical effects analysis[J]. Acta optica sinica, 2010, 30(12)：3367-3372. (in Chinese)

[15] XU L, ZHANG Z Y, CHEN X, et al. Improved sparrow search algorithm based BP neural networks for aero-optical imaging deviation prediction[J]. Journal of optoelectronics·laser, 2021, 32(06)：653-658. (in Chinese)

[16] WANG F J. Computational fluid dynamics analysis[M]. Beijing：Tsinghua University Press, 2004. (in Chinese)

[17] ZHU Z T. Analysis of aero-optical effect around the turbulent flow field of the high-speed aircraft[D]. Nanjing： Nanjing University of Science And Technology, 2016. (in Chinese)

[18] XUE D T. Engineering estimation of aero-optics imaging deviation based on backward ray-tracing[D]. Tianjin：Tianjin University of Technology, 2018. (in Chinese)

[19] LIU Y, YUAN Y T, GUO X, et al. Influence analysis of atmospheric refraction on location of television guiding missiles[J]. Acta aeronautica ET astronautica sinica, 2018, 39(12)：285-294. (in Chinese)

[20] XU L, XUE D T, LV X Y. Computation and analysis of backward ray-tracing in aero-optics flow fields[J]. Optics express, 2018, 26(1)：567-576.